# Recent advances in displacement measuring interferometry

Meas. Sci. Technol. 4 (1993) 907–926. Printed in the UK

# Recent advances in displacement measuring interferometry

**Norman Bobroff**

IBM Thomas J Watson Research Center, PO Box 218 Yorktown Heights, NY 10538, USA

Received 15 February 1993, accepted for publication 25 May 1993

**Abstract.** The present state of high-resolution displacement measuring interferometry is reviewed. Factors which determine the accuracy, linearity and repeatability of nanometre-scale measurements of displacements exceeding a millimetre are emphasized. Many aspects of interferometry are discussed, including general metrology and alignment errors, as well as path length errors caused by changes in orientation of optical components such as cube corners. Optical mixing and the nonlinear relation between phase and displacement are considered, as well as the influence of diffraction on accuracy. Where possible, quantitative measures of the effect of these parameters on performance are provided. Environmental stability is a major factor in the repeatability and accuracy of measurement. It is difficult to obtain a measurement accuracy of $10^{-7}$ when working in air. Several approaches to improving this situation are described, including multiwavelength interferometry. Recent measurements of the short- and long-term frequency stability of lasers are summarized. Optical feedback is a subtle, but important source of frequency destabilization, and methods of detection and isolation are reviewed. Other active areas of research, such as calibration of phase measuring electronics used for subfringe interpolation, are included. Progress in '*in situ*' identification of error sources and methods of validating accuracy are emphasized.

**Norman Bobroff** has been a research staff member in optics at the IBM Thomas J Watson Research Center since 1982. His current interest is interferometric displacement metrology with applications to high accuracy coordinate measurement. Mr Bobroff has also been involved in optical system testing and has constructed instruments for the quantitative evaluation of lens performance. He has participated in the development of optical alignment systems for x-ray and optical lithography. He has also been interested in scanning and alignment stages for lithography applications.

Prior to joining IBM, Mr Bobroff helped develop a spectrometer to observe stellar radiation at extreme ultraviolet wavelengths during a sounding rocket flight. Mr Bobroff received his SB at the University of Chicago and a PhD in physics from California Institute of Technology in 1983. He is active in the American Society for Precision Engineering.

## 1. Introduction

The primary objective of displacement measuring interferometry is to perform linear and repeatable measurements. These criteria are the basis of accurate measurement. The resolution of the interferometer is the minimum detectable displacement of the interferometer target. Resolution is the displacement equivalent of one standard deviation of the system noise. The dynamic range of a displacement measurement is the ratio of measurement range to resolution. Precision, as defined here, is the resolution relative to the physical size of the instrument. Many interferometric measurements require high precision, but have low dynamic range. The most extreme example is gravity wave detection. Because displacement interferometry is such a diverse field, this paper emphasizes measurement considerations for a dynamic range exceeding $10^6$, and resolution of the order of 0.1–10 nm. Applications in this regime include metrology for semiconductor fabrication, ruling of gratings and the fabrication of large optics. The advancing fields of precision robotics in medicine (Charette *et al* 1992) and stellar interferometry also require interferometric sensors of this dynamic range.

Figure 1 shows two common configurations of a modern displacement interferometer. The source is usually a polarized and frequency stabilized He–Ne (633 nm) laser. An output power of 500 $\mu$W is typical. The optical bandwidth of a mode of the laser cavity is a few megahertz. The laser output is separated into measurement and reference beams of orthogonal polarization by a polarizing beamsplitter (PBS). After returning to the beamsplitter, the measurement and reference beams are combined into a common polarization state by a linear polarizer. The beam is imaged onto a high-speed photodiode where the receiver and electronics count interference fringes. The fringe count corresponds to a variation in optical path length between the interfer-

0957-0233/93/090907+20 $07.50 

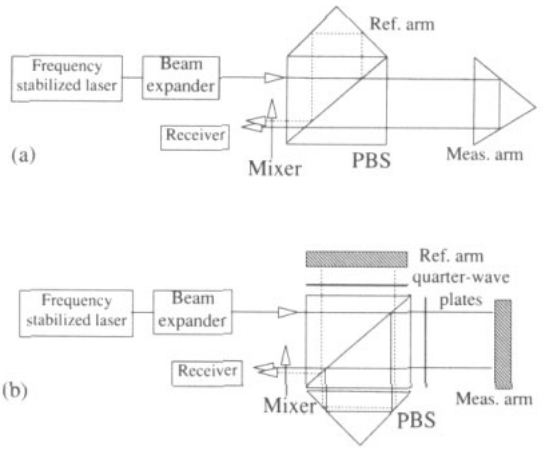


**Figure 1.** (*a*) A common configuration of a linear displacement measuring interferometer. (*b*) The plane mirror interferometer used for linear displacements with double the resolution of (*a*). Widely used for measuring *X–Y* coordinates, as discussed in section 2.

ometer arms. The optical path length (OPL) is the integral of the index of refraction along the beam path, $\text{OPL} = \int_A^B n(x, y, z)\ \text{ds}$. Thus, the OPL change measured by the interferometer results from a combination of physical displacement of an arm and environment variations which modify the index. A major difficulty in high-resolution displacement interferometry is separating these two components of OPL change.

The intensity fringes formed by each wavelength of the source bandwidth add incoherently. Because the source is not monochromatic, the fringe modulation decreases greatly at a displacement equal to the coherence length of the laser, $\lambda^2/2\Delta\lambda$. The measurement range is also limited by beam diffraction and atmospheric degradation of the interference fringes. The interferometer of figure 1(*a*), in which the beam makes one pass off the cube corner target, is used for linear displacement measurement. One fringe corresponds to a change in OPL of half the vacuum wavelength ($\lambda_v/2$). The layout of figure 1(*b*) takes advantage of the linear polarization states of the arms to obtain two passes off a plane mirror target. This layout doubles the resolution of figure 1(*a*), and is widely used in $X-Y$ coordinate measurement as discussed further in section 2. Sections 2 and 3 provide detailed consideration of the geometric and optical properties of these interferometers.

The repeatability, resolution and dynamic range of the majority of interferometric displacement measurements have improved over the last ten years. The measurement bandwidth and resolution–bandwidth product have also increased. These advances are primarily a consequence of evolving instrument technology, rather than the introduction of new concepts. An increasing awareness of the subtle sources of error in interferometry, and the principles of metrology, have also contributed to improvements in measurement. A measurement accuracy of one part in $10^7$ is about the state of the art when working in air. It is very difficult to verify accuracy at this level. A high-performance interferometric positioning system is based on many high-precision components. Many systems are not capable of measuring a traceable artefact such as a length standard. Therefore, accuracy can only be validated indirectly, by full understanding and traceable calibration of each subsystem.

This review emphasizes the advances in interferometric displacement metrology which have taken place over the last ten years. The connection between these efforts and measurement accuracy is stressed. Current research and areas in which further development is necessary are also highlighted. A more basic and broader perspective of the field of interferometry, including additional references, is provided in the review by Hariharan (1987). Table 1 summarizes the topics included in this paper from the perspective of their contribution to measurement error. The kinematic properties of displacement measuring interferometers are described in section 2. These include the effective measurement axis and cosine errors for an interferometer with different target types. Section 3 discusses the influence of optical symmetry and wavefront aberrations on the measurement linearity. Environmental factors are considered in section 4. The present state of frequency stabilized lasers is reviewed in section 5. The rapidly advancing area of phase measuring electronics is summarized in section 6. The reference list of papers on interferometry is arranged by subject. Included are publications explicitly cited in this review and supplementary sources of information.

## 2. Geometric factors in interferometric metrology

Use of a perfectly linear and accurate interferometer does not guarantee accurate displacement measurement. Misalignment and offset between the axis of the measurement transducer and the target displacement are a source of metrology error. For example, the angular orientation of the transducer axis to the target motion determines the classical cosine error. A typical in-plane metrology system which includes interferometer axes to measure pitch, roll and yaw, as well as translation, is shown in figure 2. This measurement configuration is widely used in the semiconductor metrology industry. Transducer alignment errors are complex for in-plane metrology with $X-Y$ plane mirror interferometers. Although analysis of these metrology errors is beyond the scope of this review, the transducer axis of an interferometric displacement sensor is an interesting and important concept.

Figure 3 considers more closely the geometry of the interaction of the laser beam from the interferometers of figure 1, with the retroreflector or plane mirror target. In figure 3(*a*), an interferometer measures the displacement of a retroreflector target, while in figure 3(*b*) a plane mirror target is used. The effective transducer axis is different for each of these targets. For the retroreflector target of figure 3(*a*), the displacement is determined by

**Table 1.** Summary of contents and some common error sources.

| Topics/common sources of error | Magnitude | Section of paper |
|---|---|---|
| Measurement geometry | | 2 |
| Cosine error | $\theta^2/2$ (of path) | 2 |
| Cube corner rotation | $7\theta^4$ (mm) (25 mm cube) | 2 |
| Interferometer optics | | 3 |
| Optical nonlinearity (homodyne) | $<1$ (nm) | 3.1 |
| Optical nonlinearity (heterodyne) | 4–10 (nm) | 3.2 |
| Wavefront aberration/diffraction | 1–4 (nm) | 3.4 |
| Environmental considerations | | 4 |
| Index of refraction | $10^{-6}$–$10^{-7}$ (of path) | 4.1, 4.2 |
| Contaminants, Solvents etc. | $10^{-8}$ (of path) | 4.2 |
| Air turbulence | $10^{-8}$ (of path) | 4.3 |
| Metrology lasers | | 5 |
| Short term frequency stability | $10^{-8}$–$10^{-11}$ (of path) | 5.2 |
| Long term frequency stability | $10^{-6}$–$10^{-9}$ (of path) | 5.3 |
| Accuracy frequency reference | $10^{-10}$–$10^{-11}$ (of path) | 5.4 |
| Optical feedback | | 5.5 |
| Electronics (recent developments) | | 6 |
| Phase meter linearity | $<1$–10 nm | 6 |

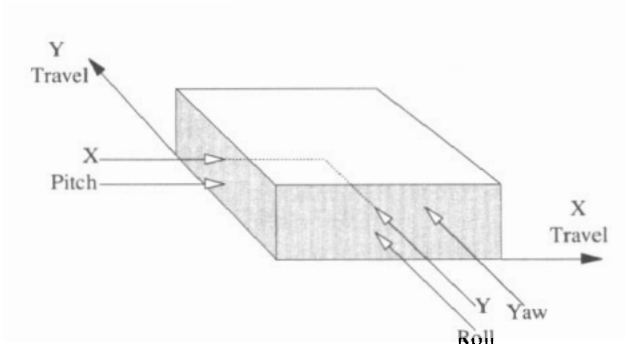


**Figure 2.** An in-plane metrology system. Five interferometer axes measure the displacement and attitude of a stage constrained to move in the $X$–$Y$ plane.

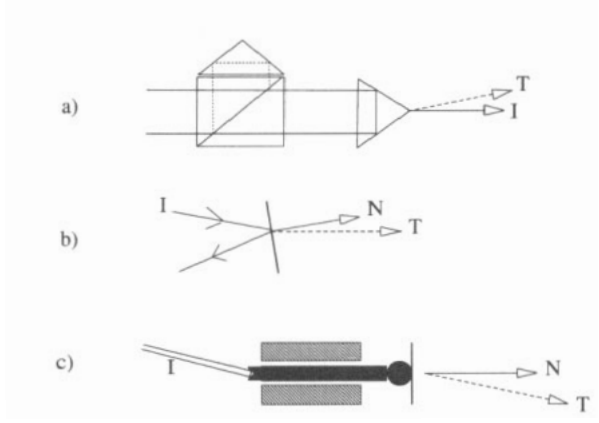


**Figure 3.** (*a*) For a retroreflector target, the travel vector ($T$) and interferometer beam ($I$) determine the measured displacement. (*b*) With a plane mirror target, the mirror normal ($N$) acts as the transducer axis. (*c*) A mechanical linear displacement probe which is equivalent to the plane mirror interferometer.

the optical path of the ray of the interferometer beam ($I$) which intersects the vertex of the cube corner. The measured displacement is the projection of the travel vector ($T$) connecting the endpoints of the vertex motion along the interferometer beam. The measured displacement is $T \cdot I$ for a hollow cube corner retroreflector. Therefore, the interferometer beam defines the transducer axis. If the target is a solid glass cube corner that rotates as it translates, refraction lengthens the path of the ray passing through the vertex. Rotation of 10°–20° occurs in some methods of writing servo tracks on disc drives. The servo tracks, which must be equally spaced, are often written using a rotary arm on which a retroreflector is mounted (see for example, 'Disk drive-servo track writing', Application Note 325-11, Hewlett Packard Corporation). In this case, it is necessary to correct the vertex motion $T \cdot I$ for the optical path (OPL) in the rotated cube corner. This correction is derived with reference to figure 4. Figure 4(*a*) shows the vertex of a cube corner, and the location of the nodal point. The nodal point is the image of the vertex as seen from outside the cube. The correction for rotation about the vertex is derived using figure 4(*b*), which unfolds the path of the ray which passes through the vertex. The path length in the rotated cube is equal to that of a plane parallel plate of glass whose thickness is twice the height ($h$) of the cube corner vertex above the entry face. In terms of the index of glass and air, the correction for rotation about the vertex is

$$\mathrm{OPL_V}(\theta) - \mathrm{OPL_V}(0) = 2h\{[(n_g^2 - n_a^2 \sin^2\theta)^{1/2} - n_a \cos\theta] - (n_g - n_a)\}. \qquad (2.1)$$

The correction in OPL for rotation about any other point is found by combining equation (2.1) with the geometric translation of the vertex. This is indicated in figure 4(*c*) for rotation of the cube about the nodal point, which is

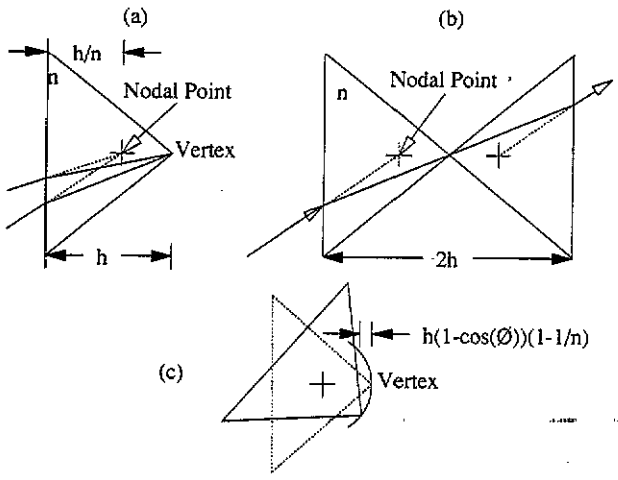


**Figure 4.** (*a*) Plan view of a solid cube corner of height $h$ and refractive index $n$. The nodal point is the apparent location of the vertex as viewed from outside the cube. (*b*) An unfolded view of the ray which passes through the vertex. The optical path is that of a plane parallel plate of thickness $2h$, as provided in equation (2.1). (*c*) When a corner cube rotates about the nodal point, the vertex also translates. Equation (2.2) gives the optical path change for rotation about the nodal point.

located $h(n_g-1)/n_g$ from the vertex. Rotation about the nodal point minimizes the refractive correction and is proportional to the fourth power of the rotation angle for small angles. The exact correction for rotation about the nodal point is

$$\mathrm{OPL_N}(\theta)-\mathrm{OPL_N}(0)=2h[(n_g^2-n_a^2\sin^2\theta)^{1/2} -(n_a\cos\theta/n_g)-(n_g-n_a/n_g)]. \quad (2.2)$$

A correction for deviation of the plane surfaces of the cube corner from orthogonality may be necessary for nanometre metrology. Deviations from ideal cube corner geometry are a consideration in achieving 0.1 nm accuracy in the metrology for stellar interferometers (Hines *et al* 1992). Another aspect of the solid cube corner, discussed in section 3, is that the reflective Fresnel phase shifts may depend on the orientation of the cube to the beam.

In figure 3(*b*), a plane mirror target replaces the cube corner retroreflector. The displacement measured by the interferometer is

$$D=(N\cdot I)(T\cdot N). \quad (2.3)$$

The factor $N\cdot I$ arises from misalignment of the interferometer beam to the mirror normal ($N$). $T\cdot N$ is the classical cosine error and is independent of the interferometer beam. Thus, the transducer axis of a plane mirror target is the mirror normal. Figure 3(*c*) shows a stylus transducer that is equivalent to the plane mirror interferometer. The contacting stylus probe has an axis $N$ defined by a journal bearing. The probe displacement is monitored by an interferometer viewing a cube corner target on the end of the probe shaft. The measured displacement is that of equation (2.3). The contrast between transducer axes for retroreflector and plane

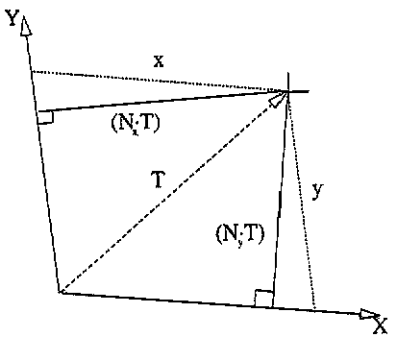


**Figure 5.** A stage is displaced along a travel vector $T$ (broken line). The component displacements measured by a linear interferometer (dotted lines) and by an $X$–$Y$ plane mirror interferometer (full lines) are shown.

mirror targets is further emphasized in figure 5. In-plane displacement of an $X$–$Y$ stage is measured by two methods. In one method, linear interferometers with retroreflector targets measure displacement along each of the non-orthogonal $X$ and $Y$ axes. The measured displacement corresponds to the projections of $T$ on the $X$ and $Y$ axes. These projections are indicated by the dotted lines labelled $x$ and $y$. In the second method, an $X$–$Y$ plane mirror interferometer, such as that of figure 2, measures the projection of stage travel along the mirror normals according to equation (2.3). This displacement is indicated by the full lines in figure 5. The difference between the two measurements is of second order in the deviation of the axis from orthogonality. A detailed discussion of interferometer transducer axes, target misalignments and associated metrology errors is available in the literature (Bobroff 1993).

## 3. Interferometer optics

When making nanometre measurements, error sources inherent to the interferometer optical system must be characterized. Optical mixing can produce a nonlinear relation between the phase of the interference fringes and the displacement. This error has a period of one fringe and a typical magnitude of 5–10 nm in commercial heterodyne interferometers. Although the potential for error from optical mixing has been known for quite some time (Bruning *et al* 1974), it is only within the last ten years that detailed attention has been given to the problem in heterodyne interferometers (Quenelle 1983, Bobroff 1987, Rosenbluth and Bobroff 1990). Homodyne interferometers are also subject to nonlinearities from optics and electronics, as discussed in sections 3.1 and 6. However, the errors achieved in practice with a homodyne interferometer have not been clearly quantified in the literature. Diffraction and wavefront aberrations are also sources of error at the nanometre level. A nanometre is only 1/600 of a wavelength for He–Ne at 633 nm, and even well-corrected optics have wavefront aberrations of $\lambda/8$. Integrally constructed metrology stages, in which the interferometer mirrors are intention-

ally rotated with the sample chuck, are increasingly common (Kendall *et al* 1991). Mirror rotation shears the interfering wavefronts (see section 3.4). Shear, in combination with wavefront aberrations or asymmetric apodization, introduces displacement errors. Recent progress in characterizing and reducing these errors is discussed below.

### 3.1. Optical mixing, polarization mixing and nonlinearity

Optical mixing refers to incomplete separation of the polarization or frequency states in a polarizing interferometer. Optical mixing is considered first for the single-frequency polarizing interferometer of figure 6. The polarization basis states of the interferometer are defined by the beamsplitter surface. The transverse electric (TE) mode is polarized perpendicular to the plane of incidence. The orthogonal state, polarized in the plane of incidence, is the transverse magnetic (TM) state. The incident wavefront is polarized 45° to the beamsplitter interface. The TM component is transmitted, while the TE state is reflected. For an ideal polarizing beamsplitter, each polarization state at the output of the interferometer consists solely of light which has propagated along a single arm. In this case, the optical phase shift between the TE and TM states is a linear function of the optical path difference between measurement and reference paths.

However, the separation of polarization states at the beamsplitter is imperfect. Ideally, the TE state incident on the receiver consists entirely of light from the reference path. In practice, this state is contaminated by a small fraction of radiation which has propagated along the measurement arm. Similar polarization mixing occurs in the TM state. The polarization states incident on the receiver are depicted in figure 7. The horizontal and vertical axes of figure 7(*a*) correspond to TE and TM mode polarizations. The electric field magnitudes for the primary and mixing components of each arm are represented by the length of the vectors along each axis. Figure 7(*b*) shows the phasor representation of each field, as well as the resultant phasor for the TE and TM states. The net TE mode phasor traces out the small dotted circle in the figure as the measurement arm moves through a fringe. The measured phase between the net TE and TM phasors leads and lags that of the pure components as the interferometer path phase ($\vartheta$) is scanned through 360° (one fringe). This results in a

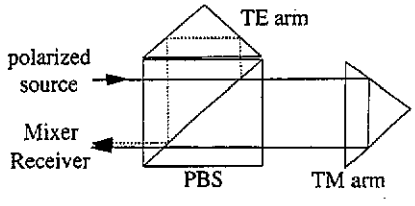


**Figure 6.** A simple polarizing interferometer which measures linear displacement.

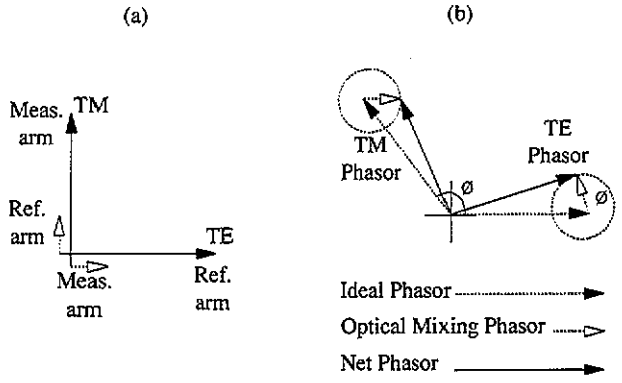


**Figure 7.** (*a*) The two horizontal vectors indicate the magnitude of the TE polarized light in the measurement and reference arms. The same quantities are shown on the vertical axis for the TM state. (*b*) The primary component (broken) and net (full) electric field phasor in each polarization state incident on the receiver are displayed. As the true phase ($\phi$) of the interferometer moves through 360°, the deviation of the net phasor from the primary component is indicated by the dotted circle (see also figure 9).

periodic measurement error. It is also clear from figure 7(*b*) that the total output intensity (the sum of the squared length of the net TE and TM phasors) varies in proportion to the phase lead or lag. Also, note that if the mixing vector is the same in each arm there is no phase error. This symmetric condition is discussed further in section 3.2. A periodic intensity modulation as small as 0.001 can be detected with a photodiode and amplifier. A homodyne receiver usually generates sine and cosine quadratures by mixing the TE and TM phasors in a quarter wave plate and linear polarizer. The signature of phase error in the total intensity can be directly applied to correct the phase error in the quadrature signals (Augustyn and Davis 1990).

In practice, polarization mixing is usually very small. Mixing is introduced by leakage at the polarizing beamsplitter and by modification of the polarization states in the arms of the interferometers. The component of beamsplitter leakage reaching the receiver passes through the beamsplitter twice. An amplitude rejection ratio of about 0.03 per pass results in a worst-case phase error of about 1 mrad. For a single-pass interferometer of figure 6, the displacement equivalent of 1 mrad is 0.05 nm. A rejection ratio of 0.03 is typical of a high-quality beamsplitter. A coating design of 30 layers may be necessary to achieve this performance, especially in the reflected beam. Imperfect or misoriented optical elements such as waveplates and cube corner retroreflectors also mix the polarization state of each arm. Tilted components, such as beam steering mirror optics, are another potential cause of polarization modification. Cube corners are particularly interesting. An excellent treatment of the polarization properties of cube corners is provided by Player (1988). Player's analytical treatment, emphasizing total internal reflection, is extended to all coatings by substituting the Fresnel relations into equation (13) of the reference. A solid cube corner retro-

reflector coated with silver, common in commercial interferometers, rotates the polarization by 0.1 rad. Of this rotated state, only 0.03 leaks through the polarizing beamsplitter. The corresponding maximum phase error is 3 mrad. The periodic measurement error introduced by polarization mixing is typically less than that associated with the phase measuring electronics. These cases are for the interferometer beam incident along the cube axis. As discussed in section 2, some applications require significant rotation of the cube corner. Depending on the coating, rotation changes the reflective phase shift and mixing, causing a systematic error in the vertex location (Hines *et al* 1992).

### 3.2. Frequency mixing and nonlinearity

The polarizing interferometer of figure 6 is often used in the two-frequency layout of figure 8. The source is either a two-frequency laser, or a single-frequency laser in combination with an acoustooptic modulator. Ideally, each frequency state is an eigenstate of linear polarization with respect to the interferometer beamsplitter. The states are separated at the polarizing beamsplitter, and a single-frequency state propagates in each arm of the interferometer. In practice, the input frequency states are elliptically polarized, and not perfectly aligned with those of the polarizing beamsplitter. Each arm contains a small component of the wrong frequency. Unlike polarization mixing, which is also present, frequency mixing is in the correct polarization state for the arm, and is not removed on returning through the polarizing beamsplitter of figure 8. After recombination at the beamsplitter, the four states of figure 8 are mixed in a linear polarizer. The resulting low-frequency components are removed by a high-pass filter. The filter cut-off is about $10^5$ fringes per second in commercial systems. Unmodulated terms are a consideration only for dynamic measurements in which data are acquired while the target is moving. The Doppler shift caused by rapid target motion may move the unmodulated terms above the cut-off frequency of the high-pass filter. The ideal heterodyne beating between the $A$ and $B$ frequency states is contaminated by two mixing terms of relative magnitude $\alpha/A$ and $\beta/B$. A comprehensive treatment of the receiver signals and resulting nonlinearity is given by Rosenbluth and Bobroff (1990). The general behaviour of the net signal is understood by representing each sinusoidal oscillation as a phasor in figure 9(*a*). The phasor corresponding to the ideal receiver beat signal has unit amplitude and phase $\Phi$. The first-order mixing terms combine to form a constant phasor of magnitude $\varepsilon$. The net phasor output formed by vector addition of the ideal and constant mixing phasor is shown in figure 9(*a*). The net phase lags and leads the true phase ($\Phi$) as the target moves through a fringe. This periodic phase error is accompanied by a proportional modulation of the amplitude of the beat frequency. The amplitude modulation ($dS$) is shifted 90° with respect to the phase error ($d\Phi$).

Frequency mixing is not a sufficient condition for nonlinearity and phase errors. If the mixing components of each arm in figure 8 have identical magnitude and phase, the phase relation between the net TE and TM phasor is unaltered. The simplest mixing mechanisms tend to produce beats in each arm that are 180° out of phase. When the single-arm beats are of equal amplitude the mixing cancels and there is no nonlinearity. This is the case when the input source states are orthogonal and the interferometer is symmetric. Two examples are a source rotated with respect to the polarizing beamsplitter, and a source with equal ellipticity in each frequency state, and principal axes at 90° (Rosenbluth and Bobroff 1990). The optical system must be asymmetric for nonlinearity to result from the optical mixing of orthagonal input states. A break in symmetry is introduced either by differential transmission of the interferometer arms or by different amounts of leakage for the two modes at the polarizing beamsplitter.

The main cause of frequency mixing and nonlinearity with a two-frequency laser source is elliptical polariz-

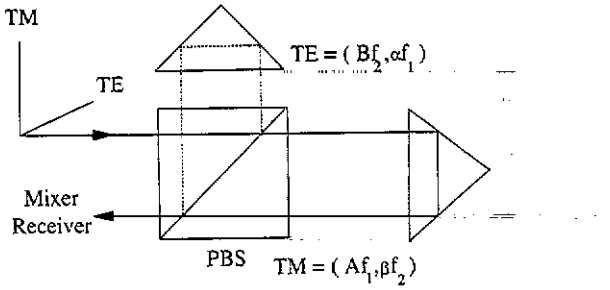


**Figure 8.** The heterodyne interferometer with frequency mixing. The amplitudes of the primary frequency components of each arm are $A$ and $B$. The contaminating frequency components have amplitudes $\alpha$ and $\beta$.

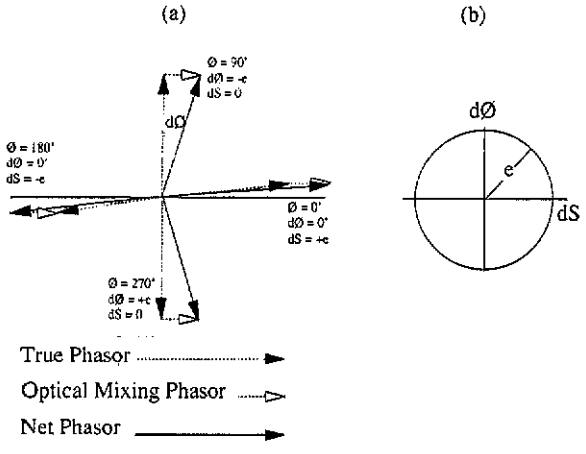


**Figure 9.** (*a*) The ideal phasor in the absence of mixing, and the contaminating phasor of amplitude $e$ and fixed orientation are shown. The receiver outputs the net phasor which leads and lags the true phase $\phi$ of the interferometer as the target is moved through a fringe or 360°. (*b*) To first order in mixing, the amplitude modulation ($dS$) of the receiver beat is in quadrature with the phase error ($d\phi$).

ation of the laser beam. Ellipticity results from birefringence in the laser cavity and head. The birefringence may vary over the life of the laser. In my laboratory, we have found that lasers which use piezoelectric transducers to tune the cavity generally have an ellipticity (the amplitude ratio of minor to major axes of the polarization ellipse) of about 0.08. The ellipses of the two frequency states are often oriented a few degrees from 90° and thus the states are non-orthogonal. It is possible that stress induced by piezo tuning causes an increase in cavity birefringence over the lifetime of the laser. The resulting nonlinearity is usually 1/30 to 1/60 of a fringe, which corresponds to a $\lambda/60$ to $\lambda/120$ displacement error for a single-pass interferometer. Laser heads which use thermal expansion to tune the cavity exhibit about an order of magnitude less ellipticity, and the principal axes of the states are orthogonal to better than 0.5°. A thermally tuned laser head combined with a symmetric interferometer optic reduces nonlinearity to less than 1/1000 of a fringe. Spurious beams of laser light reflected from optical surfaces other than the target can produce beat signals at the receiver. Stray reflections are usually prevented from reaching the receiver by small tilts of the optical components.

Frequency mixing and nonlinearity can be detected without disturbing the basic interferometer. Frequency mixing produces a beat signal at the receiver from a single interferometer arm. Individual beat signals from each arm add linearly at the receiver to the much larger beat signal between the arms. As the target is displaced, the relative phase of the interarm heterodyne beat varies with respect to the smaller mixing in each arm. The resulting modulation of the beat envelope is an unambiguous signature of nonlinearity. The beat envelope modulation is shown as a function of phase error in figure 9(*b*). Most commercial receivers supply an amplitude-demodulated output to indicate signal strength (Hewlett Packard model 10780 for example). This signal typically exceeds 500 mV, and the amplifier circuit usually saturates above 1000 mV. A 1 mV modulation at 100 Hz, corresponding to a phase error of 2 mrad, is easy to identify as the target is scanned 100 fringes per second. Preferably, the direct output of the receiver photodiode is monitored at a test point located on the emitter follower transistor connected to the photodetector.

The asymmetric component of system error can also be identified by using two receiver and phase meter channels with a 180° relative shift in optical phase. Figure 9(*a*) shows that the nonlinearity is asymmetric about 180°. The phase difference between these two signals is the asymmetric part of the system nonlinearity. Optical signals separated by 180° are produced by mixing the wavefront in linear polarizers with a 90° relative orientation. The primary caveat in this approach is that error in the phase meter is indistinguishable from nonlinearity in the interferometer. The phase meters must be independently calibrated. Some interesting work in this area is reported by Hou and Wilkening (1992). In my laboratory, the methods are combined. The modulation of the beat envelope is used to identify the optical nonlinearity. A comparison of two phase meter processing signals from the same interferometer is used to evaluate the accuracy of the phase meters. Because the nonlinearity averages to zero over a fringe, it can also be removed in low-bandwidth applications by dithering one arm of the interferometer and averaging phase readings (Hines *et al* 1992).

### 3.3. Non-polarizing interferometers

The nonlinearity of polarizing interferometers has stimulated some interest in non-polarizing interferometers. These are implemented as either single-frequency or two-frequency instruments. An example of a heterodyne non-polarizing interferometer with negligible nonlinearity is given by Tanaka *et al* (1989). The non-polarizing, heterodyne interferometer has several disadvantages. Much of the flexibility of polarizing optics, such as the two-pass plane mirror interferometer of figure 1(*b*), is compromised. A large number of optical components must be aligned and free of mechanical drift. Modern versions of the single-frequency, non-polarizing interferometer, which dates back to A A Michelson, have also been developed. Optically generated quadratures are created to obtain high-resolution subfringe interpolation. For example, the 90° phase shift between the TE and TM state fringe patterns can be produced by a $\lambda/8$ plate situated in the reference arm (Downs and Raine 1979). A 90° phase shift is also obtained by a specially designed absorbing metal film beamsplitter coating. Parasitic phase shifts may be introduced by other optical elements such as retroreflectors. The quadrature signals must be carefully analysed to determine their precise phase relation, and to adjust the detector gains and offsets (Downs and Raine 1979, Heydemann 1981).

Subfringe interpolation based on the spatial rather than temporal interference pattern is revisited by several recent studies. The fringe pattern obtained from the interference of the measurement and reference beams at a small angle is projected on an array of photodetectors. Each array element is separated by 120° of phase. This technique lends itself to high-bandwidth, high-resolution fringe interpolation, as demonstrated by Mertz (1983, 1988, 1989) and Hagiwara *et al* (1989). However, the spatial fringe pattern is a function of target position because of wavefront curvature and perhaps higher diffraction orders of the interfering beams. This technique is most promising for interferometric read-out of glass scales, or angle measurement where the path change of each beam is small. As with all unmodulated interferometers, the calibration and stability of electronic gains and offsets is a concern.

### 3.4. Diffraction

There are two important properties of interferometer wavefronts. In this case, aberration is the deviation of a wavefront from planarity. Apodization is the variation in intensity across a wavefront. A truncated Gaussian

apodization is characteristic of the fundamental transverse cavity mode ($TEM_{00}$) used in metrology lasers. The wavefronts are spherical with a radius of curvature which varies with distance from the waist according to the well-known equations of Gaussian beam propagation. The influence of diffraction on linearity and accuracy is difficult to quantify and identify. An excellent treatment of the effect of Gaussian and astigmatic wavefronts on interferometric accuracy is given by Monchalin in the context of precision wavelength measurement (Monchalin *et al* 1981). A purely Gaussian beam changes the scale, or effective wavelength, of the interferometer by about $10^{-12}$ for a 633 nm He–Ne laser with a 300 $\mu$m beam waist. The scale change increases with the square of the wavelength, and is of consideration in stellar interferometry where longer wavelength interferometers are used to reduce scattered light in the optical system.

In most applications, the aberration and apodization of the beam are difficult to measure or predict. The Gaussian beam emerging from the cavity is often enlarged by a beam expander 'telescope' in the laser head. In commercial laser heads (such as Zygo Axiom) the beam at the exit of the expander has a 1/e diameter of 3–6 mm, compared with about a 0.3 mm beam waist in the laser cavity. The cavity waist is imaged 15–20 m from the laser head. The 'telescope' is usually designed to fit in a small space and contains an optical element of large numerical aperture. Even well-made optics introduce $\lambda/8$ aberrations. Interferometer optics also consist of a large number of interfaces at nominally planar surfaces which further degrade the beam. If the beam lands on the joint of a cube corner, both the intensity and symmetry of the beam are reduced. In applications such as disc track writing, it can be difficult to avoid the joint because the retroreflectors are small. The issue of aberration and apodization is especially relevant to modern stage technologies in which the plane mirror targets of figure 2 rotate with the stage (Kendall *et al* 1991). As shown in figure 10, rotation introduces a shear between the measurement and reference wavefronts. The shear varies as the stage translates, causing the average phase of the interfering wavefronts to change.

Aberrated or apodized wavefronts can be identified by limiting the portion of the beam imaged onto the detector. For example, an aperture of 1–2 mm diameter is placed in front of the receiver so that only a portion of the 6 mm beam is transmitted. Changes in the phase meter output which occur as the aperture is translated across the beam indicate aberrated wavefronts. I have observed phase shifts of 30° with this approach. Because the receiver averages the wavefront over the full aperture, the range of observed phase shifts provides an upper limit to the actual interferometer errors.

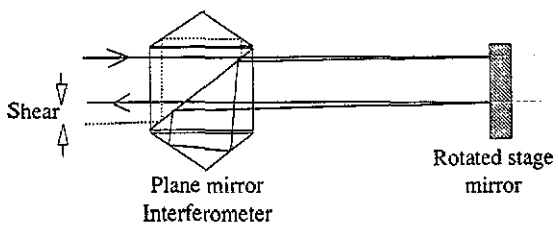


**Figure 10.** Some stages used in semiconductor lithography rotate the plane mirror interferometer target more than 20 mrad to adjust the orientation of a wafer. This rotation shears the interfering measurement and reference wavefronts.

## 4. Environment

Interferometer electronics accumulate the total change in fringe count ($F_{acc}$) relative to a reset position. The fringe count measures the change in optical path length (OPL) in units of the vacuum wavelength ($\lambda_v$) so that $OPL = F_{acc}\lambda_v$. Variations in the environment cause the refractivity $(n-1)$ and fringe fraction to change, even when the physical displacement of the interferometer target is zero. The correction for environmental changes in fringe fraction is termed *compensation*. The corrected fringe fraction corresponds to the component of OPL change due solely to physical displacement of the target. Compensation is a key aspect of metrology in air. The refractivity of air is large, and depends strongly on temperature and pressure. Furthermore, the thermal conductivity of air is low, making it difficult to achieve a homogeneous thermal environment. Optical components of the beam path such as beamsplitters, retroreflectors and waveplates also have high refractivity and poor thermal conductivity. These properties, summarized in table 2, are obstacles to repeatable and accurate measurement at the $10^{-7}$ level. The thermal properties of borosilicate glass (BK7) and fused silica, commonly used in optical components, are also included in table 2.

Traditional methods of compensation assume that the environment is homogeneous and varies slowly with respect to the thermal time constants of the optics. These techniques, which typically utilize environmental data from one location to infer the refractivity everywhere, are summarized in section 4.2. However, many environments are not sufficiently homogeneous or quasi-static to apply these methods. An important research area is compensation of environments where air flow introduces significant refractivity fluctuations. This situation arises in semiconductor metrology where a substantial flow of filtered air is used to reduce particulate contaminants. Multiwavelength displacement interferometry is a potential solution to this problem, and recent results are summarized in section 4.3.

### 4.1. Compensation

The physical location of the starting or zero point of an interferometric measurement is monitored by the optical path rather than physical path length. Variations in ambient conditions cause changes in the OPL, and hence in the fringe count corresponding to the zero point. This is the perspective of figure 11, in which an environmental change has caused an apparent shift of d$F$ fringes in the zero point. Compensation maintains a stationary zero

**Table 2.** Properties of optical path media.

| | Air | He | BK7 | Fused silica |
|---|---|---|---|---|
| $(n-1)$ 633 nm, dry, STP | $271.8\times10^{-6}$ | $30\times10^{-6}$ | 0.51 | 0.42 |
| $dn/dT$ ($K^{-1}$) | $1.0\times10^{-6}$ | $1.1\times10^{-7}$ | $1.5\times10^{-6}$ | $10.0\times10^{-6}$ |
| $dn/dp$ ($Pa^{-1}$) | $2.7\times10^{-9}$ | $3.0\times10^{-10}$ | – | – |
| Expansion ($K^{-1}$) | – | – | $8.0\times10^{-6}$ | $0.6\times10^{-6}$ |
| 1/OPL d(OPL)/d$T$ ($K^{-1}$) | $1.0\times10^{-6}$ | $1.1\times10^{-7}$ | $3.7\times10^{-6}$ | $6.7\times10^{-6}$ |
| Conductivity (mW $m^{-1}$ $K^{-1}$) | 26 | 150 | $1.5\times10^{3}$ | $1.4\times10^{3}$ |

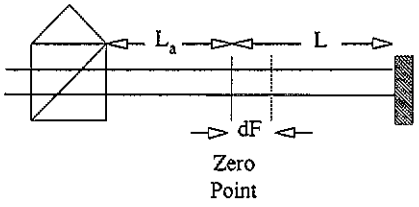


**Figure 11.** The interferometer is zeroed at a physical location in space (zero point). The interferometer measures optical path length rather than physical path. Thus, the apparent location of the zero point may drift by d$F$ fringes with changes in refractivity of the propagation medium.

or reset position in space by correcting the accumulated fringe count for the environmental changes. The correction in fringes (d$F$) for a homogeneous environment at time ($t$) is computed in terms of the air ($n_a$) and glass ($n_g$) indices, and thermal expansion ($\alpha$ d$T$) by

$$\lambda_v\, dF = L_g[(n_g(t)-n_g(0))+(n_g(t)-1)\alpha\, dT] + L_a(n_a(t)-n_a(0)). \quad (4.1)$$

$L_g$ is the difference in physical glass path between the measurement and reference arms at the physical zero location. $L_a$ is the corresponding difference in the air path. The corrected fringe count, corresponding to actual target motion, is

$$F_{cor} = F_{acc} - dF. \quad (4.2)$$

The physical displacement of the target ($L$) is given in terms of the current wavelength by

$$L = F_{cor}\lambda_v/n_a(t). \quad (4.3)$$

A common oversight in compensation is to ignore the component of the optical path in glass ($L_g$). For example, the measurement arm of the standard plane mirror interferometer (figure 10) contains two more beamsplitter cube passes and four more waveplate passes than the reference arm consisting of a single cube corner. The unbalanced optical path exceeds 120 mm for a 35 mm beamsplitter cube and a 3 mm thick waveplate. As noted in table 2, the thermal coefficient of OPL change for BK7 glass is about four times that of air. Also, glass may not change temperature as rapidly as air and is likely to have thermal gradients. It is important to minimize $L_g$ by using symmetric configurations of the interferometer in which the internal beam paths of measurement and reference arms are nearly identical. A combination angle and displacement interferometer which is highly symmetric and very compact is described by Sommargren (1987, 1989). Most differential interferometers have nearly common internal measurement and reference beam paths (Baldwin and Siddall 1984, Sommargren 1987). Steinmetz compares the environmental thermal sensitivity of several interferometer optical systems (Steinmetz 1988). His study reports nanometre stability for a differential interferometer, despite ambient temperature variations of 4°C per hour. The optical properties of components such as wave plates are also temperature-dependent. For example, the phase between nominal sine and cosine quadratures in a polarizing interferometer is temperature-dependent.

### 4.2. The refractivity of air

Compensation requires regular updates of the refractivity. In most applications, indirect measurements of refractivity are used. These are based on the ambient temperature, pressure, relative humidity and $CO_2$ concentration. The index of refraction is a linear function of these environmental parameters over moderate excursions from the initial conditions. The first order coefficients of index variation for air and glass are provided in table 2. When repeatable displacement measurement is required, it suffices to evaluate index changes based on a linear parametrization of refractivity. In this case, an error in absolute value of the index causes a scale error in equation (4.3). The exact value of the ambient refractivity is necessary for an accurate displacement measurement. The refractivity of air is well approximated by the product of a dispersion relation depending only on wavelength, and a density function parametrized by temperature, pressure and composition, notably water vapour and $CO_2$. An extensive development and review of the accuracy of this two-component description is provided by Edlen (1966). Edlen's widely used formulae for the index of refraction are summarized in the first four rows of table 3. Edlen estimates an accuracy of a few parts in $10^8$ over a spectral region from the far ultraviolet to the near infrared. Edlen's equations are essential to metrology and spectroscopy. The experimental uncertainty in these relations has been reduced by recent measurements using direct refractometry (Birch and Downs 1988, Birch *et al* 1988a,b, Schellekens *et al* 1986). These studies suggest a small error in the humidity term of Edlen's dispersion relation

**Table 3.** Edlen's formulae.

| Relation | Symbol | Expression |
|---|---|---|
| Edlen index; $\sigma = 1/\lambda$, Dry air, 15°C, 101.3 kPa | $(n-1)_s$ | $\left(8342.13 + \frac{2406030}{130-\sigma^2} + \frac{15997}{38.9-\sigma^2}\right) \times 10^{-8}$ |
| Edlen index as above, $x = CO_2$ concentration | $(n-1)_{sx}$ | $(n-1)_s[1 + 0.540\ (x - 0.000300)]$ |
| Edlen index Dry air $T$ (°C), $P$ (Pa) | $(n-1)_{tp}$ | $(n-1)_{sx}\frac{P}{96095.5}\left(\frac{1 + P(6.128 - 0.09976T) \times 10^{-9}}{1 + 0.0036610T}\right)$ |
| Edlen index $h$ = partial pressure $H_2O$ (Pa) | $(n-1)_{tph}$ | $(n-1)_{tp} - h(0.042922 - 0.000343\sigma^2) \times 10^{-8}$ |
| Downs' humidity correction | $(n-1)_{tph}$ | $(n-1)_{tp} - h(0.037209 - 0.000343\sigma^2) \times 10^{-8}$ |
| 633 nm, $T$ (K), $P$ (Pa) $H$ = % relative humidity | $(n-1)_{tpH}$ | $271.8 \times 10^{-6}\left(\frac{P}{101325}\right)\left(\frac{293.15}{T}\right)[1 + 0.54(x - 0.000300)] - 10^{-8}H$ |

(Birch and Downs 1988). This correction at the $10^{-8}$ level is generally recognized by the metrology community, and has been experimentally verified (Beers and Doiron 1993). Downs' humidity term is included in table 3. Jones reviews the relation between density of air, equation of state and composition, using recent experimental data. The results of this work are compared and combined with Edlen's dispersion relation (Jones 1981). Jones' parametrization of the density differs slightly from Edlen's. However, both agree within the experimental error of compensation in open air. Jones' paper contains several useful approximations to the density and index equations which are accurate to $10^{-7}$ within 10 K and 30 kPa of standard conditions. A convenient approximation to Edlen's equation is included as the last entry of table 3. It is valid to a few parts in $10^8$ in the range 285–300 K, and 90–110 kPa. The approximation uses the relative humidity ($H$), rather than the partial pressure of water vapour ($h$). The relative humidity at high elevations should be adjusted to that at sea level.

Compensation based on a limited number of environmental factors is subject to error in the presence of contaminants. In practice, $CO_2$ concentrations are rarely monitored. The present atmospheric $CO_2$ concentration is 355 ppm, and increases by about 2 ppm per year. It is not uncommon for the concentration to be several times greater in the presence of people. The refractivities of some common laboratory chemicals are included in table 4 (provided courtesy of G Wilkening, PTB). Although some of these chemicals are highly refractive, metrology environments are usually free of these vapours. Many are detected by odour at levels that cause an index change of $10^{-7}$. An extensive list of the minimum detectable contaminant concentrations by smell is compiled by Ruth (1986). Humans can detect 1 ppm of ethyl alcohol and 20–40 ppm of acetone.

A refractometer directly measures the index by interferometric monitoring of the change in OPL of a known path which is alternately evacuated and filled with air. Direct refractometry is used to measure the refractivity and density of chemical species in non-standard environments. It is occasionally applied to compensate metrology interferometers, especially if absolute accuracy is essential or contaminants are suspected. However, for most applications, the slow speed, spatial isolation and high cost of the refractometer are major drawbacks. The plumbing and optical paths of the refractometer are long and narrow, with a high ratio of surface area to volume. Surface adsorption and outgassing are potential sources of systematic error. It is very difficult to verify the performance of a single refractometer. In a recent study, refractometers from several national metrology laboratories performed simultaneous measurements on a common air sample (Schellekens *et al* 1986). Despite a well-controlled experiment, it was difficult to obtain agreement to within $5 \times 10^{-8}$. The statistical error of each instrument is claimed to be about $10^{-8}$. The primary source of discrepancy was found to be surface adsorption in the air intake plumbing of the refractometers. The work of Schellekens *et al* also verified Edlen's equations with Downs' humidity correction to $5 \times 10^{-8}$.

A wavelength tracking interferometer monitors the

**Table 4.** Refractivity of some common chemicals.

| Chemical | Refractivity (at STP) $(n-1) \times 10^4$ | Contamination level (ppm) for $10^{-7}$ change in index |
|---|---|---|
| Acetone | 10.2 | 130 |
| Air | 2.72 | – |
| Ammonia | 3.5 | 1300 |
| Benzene | 15.8 | 77 |
| Carbon dioxide | 4.2 | 680 |
| Carbon disulphide | 13.5 | 93 |
| Carbon monoxide | 3.2 | 2100 |
| Chlorofluorocarbons R12 | 10.3 | 130 |
| Ethane | 8.1 | 190 |
| Ethyl acetate | 13.0 | 97 |
| Hydrocyanide | 4.0 | 780 |
| Hydrogen sulphide | 5.9 | 315 |
| n-butane | 12.9 | 198 |
| n-propane | 10.3 | 130 |
| Nitrogen dioxide | 4.7 | 510 |
| Octane | 23.0 | 50 |
| Sulphur dioxide | 6.3 | 280 |
| Tetrachloroethylene | 18.7 | 63 |

optical path length of an open cavity fabricated from a thermally stable material such as Zerodur. Wavelength tracking is an attempt to overcome the low update rate and spatial isolation of the direct refractometer. The cavity receives continuous air flow from the interferometer being compensated. The repeatability of wavelength tracking is limited by the interferometer resolution and the environmentally induced changes in cavity length. A study directly comparing wavelength tracking with compensation by measuring $T$ and $P$ reports agreement to a few parts in $10^7$ (Steinmetz 1988). Wavelength trackers are expensive, and short term performance is often improved more economically by investing in improved thermal control. Note that both refractometers and wavelength trackers are subject to all other errors in interferometry, including nonlinearity.

Validating the accuracy and repeatability of a compensation system is a significant undertaking. An interesting example is the international comparison of refractometers mentioned above (Schellekens *et al* 1986). Another example is the validation metrology developed for the large-optics diamond turning machine at Lawrence Livermore National Laboratories (Estler 1985). Interferometers in vacuum and air monitor the optical path length to a common mirror 6 m away. The air path is compensated by measuring $T$, $P$ and $H$, and applying Edlen's equations. A linear array of thermistors monitors the air temperature along the path. Thermistors are selected because of they have a high responsivity near standard temperature, typically 500 $\Omega$ $K^{-1}$. Periodic absolute calibration of thermistors is required because a reliable data base on the long term stability of thermistors is not available. Other issues associated with temperature sensors, such as self-heating and time response are discussed in the literature (Downs *et al* 1990). Ambient pressure is the environmental variable with the greatest excursion during this evaluation. The temperature was controlled to within about 40 mK. The demonstrated repeatability of compensation is about $10^{-8}$ and the accuracy is $10^{-7}$. A small and repeatable discrepancy with Edlen's equation at the $10^{-8}$ level is suggested by Estler. This discrepancy is most likely resolved by Downs' correction to the humidity term in Edlen's dispersion relation.

### 4.3. Inhomogeneous environments and multiwavelength interferometry

Many metrology environments require very clean air. Low particulate contamination is achieved by maintaining a substantial flow of filtered air, usually exceeding 100 linear feet per minute. Air flow causes density fluctuations and local variations in refractivity. It is difficult to quantify the effects of air flow in a way that applies to a general environment. Limited data are reported in the literature. One experiment observes fluctuations along a 200 mm measurement path for a static environment and several airflow rates (Bobroff 1987). Fluctuations of about 0.2 nm $mm^{-1/2}$ at one standard deviation are reported for an airflow of 100 linear feet per minute. Correlation of index fluctuations between adjacent interferometers is a quantitative measure of the index homogeneity. The correlation seems to have two spatial scales. A high (>90%) correlation which decreases rapidly with separation is exhibited for spacings less than 8 mm. A slower rate of decrease in correlation occurs at larger beam separations. An 80% correlation exists between passes of a commercial plane mirror interferometer with 12 mm beam spacing. Fluctuations introduced by high airflow are usually much smaller than the index variation introduced by a heterogeneous thermal environment. In most situations, it is preferable to maintain substantial airflow to promote thermal uniformity. In a few metrology environments, index fluctuations from air flow are starting to encroach on the system error budget. Further characterization of metrology environments is essential to understanding the limits to compensation. Finally, note that an inhomogeneous index causes bending of the laser beam. Atmospheric bending of the laser beam may be a factor in straightness measurements. In a dynamic environment with rapidly varying gradients, beam wander reduces the fringe contrast and signal-to-noise at the receiver.

The contributions to optical path change caused by target displacement and refractivity changes can be distinguished using multiple wavelength displacement interferometry. In this approach, the optical path is monitored at two or more wavelengths with significantly different indices of refraction. In principle, index variations from all sources except unknown contaminants are corrected. Significant improvements in measurment have been demonstrated in geophysical applications over air paths of several kilometres (Slater and Huggett 1976). However, there are challenges in applying this technique to nanometre metrology over ranges of less than a few metres.

The measured optical path length ($L_i$) and corresponding accumulated fringe fraction ($F_i$) at the $i^{\text{th}}$ wavelength due to actual target motion ($L$) and refractivity variation are given by

$$L_i = \hat{\lambda}_{iv} F_i / n_i(t) = L + L_a(n_i(t) - n_i(0))/n_i(t). \qquad (4.4)$$

The nomenclature follows that of equation (4.1) and figure 11, and the glass path has been neglected. When changes in the partial pressure of water vapour are small, refractivity is proportional to density so that $n_i(t) - 1 = \alpha_i \rho(t)$ (see table 3). In this limit, measurements at two wavelengths suffice to isolate the index change from the target motion $L$. When water vapour is a significant factor, three wavelengths are necessary, including one in the microwave (Slater and Huggett 1976). With the approximation $n - 1 \ll 1$, the two-wavelength solution and statistical error in target motion correction $\delta L$ are

$$n_i(t) - n_i(0) = \Gamma(L_2 - L_1)/L_a \qquad (4.5)$$

$$L = L_1 - \Gamma(L_2 - L_1) \qquad (4.6)$$

$$\delta L = (\Gamma - 1)[(\delta L_1)^2 + (\delta L_2)^2]^{1/2}. \qquad (4.7)$$

The parameter $\Gamma$ is a measure of the dispersion between

two wavelengths,

$$\Gamma = (n_1 - 1)/(n_2 - n_1). \tag{4.8}$$

Because of the low dispersion of air, a wide separation in wavelengths is necessary to obtain a small $\Gamma$. Typical values are $\Gamma = 8$ between 244 and 488 nm and $\Gamma = 17$ between 633 nm and 1.06 $\mu$m. Large values of $\Gamma$ amplify the statistical error in each interferometer (equation (4.7)). Two-wavelength interferometry is most useful when the environmental variations in OPL exceed the statistical errors by a factor of about 20. This is often the case in low-bandwidth measurement where the statistical errors are highly averaged.

Ishida describes a two-wavelength interferometer based on the argon ion laser at 488 nm (Ishida 1989). By frequency doubling in a nonlinear crystal, a coincident beam at 244 nm is produced. Environmental fluctuations of 20–50 nm are corrected to within a few nanometres. The fluctuations in the individual wavelength data are increased by about a factor of two in the corrected data. If these fluctuations were caused by electronic noise, then equation (4.7) would predict a greater amplification in the corrected data than is observed. Thus, the measurement fluctuations at high frequency must be caused by index fluctuations. It would be interesting to correlate the corrected data with those of the individual interferometers to separate the index fluctuations from the electronic noise. In another interesting experiment, Matsumoto directly compares two-wavelength interferometry (633 nm and 1.06 $\mu$m) with compensation based on temperature, pressure and Edlen's equations (Matsumoto *et al* 1992). Both methods agree to $10^{-7}$ over a 235 m path. Estler also achieved better than $10^{-7}$ with compensation based on Edlen's equation. Multiwavelength interferometry will probably be useful for long air paths where the index fluctuations exceed the amplified statistical noise in the corrected data.

## 5. Lasers and wavelength stability

The fractional repeatability and accuracy of the vacuum wavelength of the laser ultimately determine that of the displacement measurements. Most applications require the repeatability as a fraction of total displacement to be $10^{-7}$ or greater. The lower end of this range is about the limit for working in the open air, and corresponds to 10 nm measurements over a 100 mm path length. Measurements at standards laboratories may require accuracy or repeatability of the order of $10^{-9}$. The laser stability should exceed the measurement objective by more than three standard deviations. Stabilization signatures can be derived from the gain curve, an external atomic transition, or an external spectrometer or reference cavity. Gain curve stabilization is the most widely taken approach, while an external transition lock provides the highest wavelength repeatability, though at the expense of output power (see section 5.4). An external cavity or dispersive spectrometer is rarely used to stabilize a gas laser in a metrology application. However, this approach may be required to stabilize diode lasers, as discussed in section 5.6. An excellent review of stabilized gas lasers is provided by Wallard (1973). The short term frequency stability of stabilized lasers is well characterized and summarized in section 5.2. Recent work centres on the long term stability of lasers, and is covered in section 5.3. One objective is to develop a laser other than the iodine-stabilized laser that can serve as a portable secondary frequency standard with an accuracy in the $10^{-9}$ regime. Another area of interest is to increase the power and split frequency of Zeeman lasers to allow higher target velocity (for example, Hewlett Packard model 5527C). '*In situ*' detection of frequency destabilization caused by optical feedback is another important objective (section 5.5). Recent developments are illustrated mostly in the context of the He–Ne 633 nm laser. However, similar physical principals apply to most types of gas laser. Solid-state lasers are discussed in section 5.6.

### 5.1. General principles of gain-curve-stabilized lasers

The central component of most gain-curve-stabilized lasers is the integrally constructed discharge tube and optical cavity. Integral construction decreases the sensitivity of the laser to acoustics, shock and thermal drift. A 633 nm He–Ne laser tube is filled with a 9 : 1 ratio of $^3$He to Ne, at a pressure of 500 Pa (4 Torr). $^3$He is slightly more efficient than $^4$He at collisionally pumping the neon transition. As the design of the laser tube has developed, the volume of the gas reservoir has decreased relative to the discharge volume so that the lasers are more compact. Improvements in the metal-to-glass seals have caused the rated lifetime to remain roughly constant, despite the decrease in gas volume. The pressure decreases over the life of the tube, and the laser fails when the pressure is about 250 Pa (2 Torr). The lifetime rating of a typical commercial tube is 20 000 h running time. In addition to microleaks, sputtering of the aluminium anode decreases the tube pressure by trapping gas atoms on the surfaces of the laser tube. The rate of sputter pumping depends on the treatment of the anode during fabrication. No systematic study of sputter pumping, microcracks and causes of laser failure has been undertaken.

Neon has two naturally occurring isotopes, $^{20}$Ne and $^{22}$Ne. The line centre of the 633 nm $^{22}$Ne transition is about 850 MHz higher than the $^{20}$Ne transition. Within the last eight years, pure $^{20}$Ne has become the most common amplification medium for metrology lasers. The centre frequency of the atomic transition in a laser tube is shifted from the vacuum value by the gas pressure and composition. The coefficient of atomic transition change with pressure is about +135 kHz Pa$^{-1}$ (18 MHz Torr$^{-1}$). Thus, it is reasonable to expect a frequency decrease of 30–40 MHz, or one part in $10^7$, over the life of the tube. The gas pressure also depends on the temperature of the tube, which is sometimes biased above room temperature to control the tube

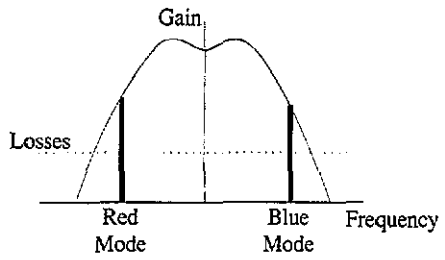


**Figure 12.** A simplified view of the gain curve of a single isotope, He–Ne laser. The depth of the Lamb dip at the line centre is exaggerated. The laser oscillates when the gain exceeds the cavity losses indicated by the dotted horizontal line. As the cavity length is changed, the cavity modes are tuned across the gain curve. Many gain-curve-stabilized lasers utilize two simultaneously oscillating modes to provide a cavity tuning signature. The orthogonal polarization of the modes is used to separate them.

length as discussed below. A correlation between tube temperature and line centre frequency has been observed (Sasagawa and Zumberge 1989).

Laser amplification occurs over the transition linewidth where the cavity gain exceeds the losses. Figure 12 shows an idealized single-isotope gain curve, with a horizontal line indicating the cavity losses. The width of the gain profile is dominated by inhomogeneous Doppler broadening of about 1.3 GHz. Homogeneous pressure broadening contributes 100 MHz to the width. A single-isotope laser exhibits a Lamb dip about 25 MHz wide, and 5–10% deep.

The laser cavity oscillates over about a 1 MHz frequency band. The oscillation wavelength is determined by the phase condition in which an integral number of wavelengths (the mode number) fit in the cavity length. Most techniques of gain-curve stabilization utilize two non-degenerate states that oscillate simultaneously, as indicated in figure 12. The intensity or frequency difference between modes is used as a feedback signature to control the cavity length. At a fixed cavity length, the wavelength of each state is inversely related to the refractivity of the cavity. However, the refractivity seen by one state depends on the frequency and amplitude of the other state. Frequency interactions between modes are an important phenomenon in the tuning characteristics of the beat frequency stabilization techniques which are described more in section 5.3. In general, as the cavity quality increases, the states try to move together because the population inversion is decreased (hole burning) and both states tend to see the same index. As a consequence, the split frequency between states varies inversely with the cavity quality (Balhorn *et al* 1975). This makes it difficult to obtain simultaneously high split frequency and output power in the axial field Zeeman lasers widely used in commercial heterodyne interferometers. Frequency pulling of the line centre also results from optical feedback into the cavity.

The cavity is tuned by varying its length. Thin film heating foils have largely replaced piezoelectric actuators for this purpose. Because piezoelectric actuators stress the tube, they can change the polarization properties of the cavity. As noted in section 3.2, piezoelectric modulated tubes tend to exhibit a greater ellipticity than thermally stabilized tubes. Variations in polarization sensitive loss ('dichroism') and birefringence differentially change the intensity of each oscillating state. This shifts the lock point in a laser stabilized for equal intensity in each state. Other locking techniques minimize the intermode beat frequency. Variable dichroism changes the intermode beat frequency and moves the lock point. Thermally stabilized tubes are biased 20–40°C above ambient to increase the bandwidth of the thermal control system. Frequency control servo bandwidths exceeding 100 Hz are reported for thermally stabilized lasers (Niebauer *et al* 1988). Differential expansion of materials in a thermally modulated tube can also change the polarization properties. One commercial manufacturer maintains constant temperature on the output mirror to minimize long term changes in dichroism (Laboratory for Science, Berkeley, CA). Further quantitative study of the origin and influence of cavity dichroism on long term frequency stability is needed.

Because many different gas mixtures, pressures and stabilization techniques are used, output frequency can vary significantly between lasers. Table 5 lists the nominal oscillation frequencies for some commercial lasers. The table illustrates the variability in wavelength between different types of He–Ne laser. Where noted, tubes contain $^{22}$Ne, or an isotope mixture which shifts the profile to the blue.

### 5.2. Short term frequency stability

Frequency stability on time scales less than 1000 s is specified in terms of the square root of the Allan variance (Allan 1966, Wallard 1973). Allan variance is the variance of the laser frequency averaged over a period $\tau$. The Allan variance is sometimes referred to as the two-sample frequency average. Short term frequency stability is affected by phase fluctuations during amplification, as well as by mechanical and thermal perturbations of the cavity. During closed loop operation, noise generated in the frequency servo electronics also influences the stability. The Allan variance of a locked laser usually exhibits

**Table 5.** He–Ne 633 nm ($^{20}$Ne unless indicated otherwise).

| Line | $f$ (MHz) | $\lambda$ (nm) |
|---|---|---|
| $^{127}I_2$ g hyperfine line | 473 612 340.4 | 632.991 302 2 |
| $^{127}I_2$ i hyperfine line | 473 612 214.7 | 632.991 398 2 |
| HP 5517A/B | 473 612 234 | 632.991 372 |
| HP 5517C | 473 612 247 | 632.991 354 |
| Zygo Axiom | 473 612 123 | 632.991 520 |
| Excel Precision | 473 612 175 | 632.991 450 |
| Laboratory for Science (200) | 473 612 050 | 632.991 618 |
| Laboratory for Science (220) | 473 612 200 | 632.991 418 |
| CMX | 473 612 310 | 632.991 271 |
| Rowley $^{22}$Ne (Rowley 1990) | 473 612 702 | 632.990 747 |

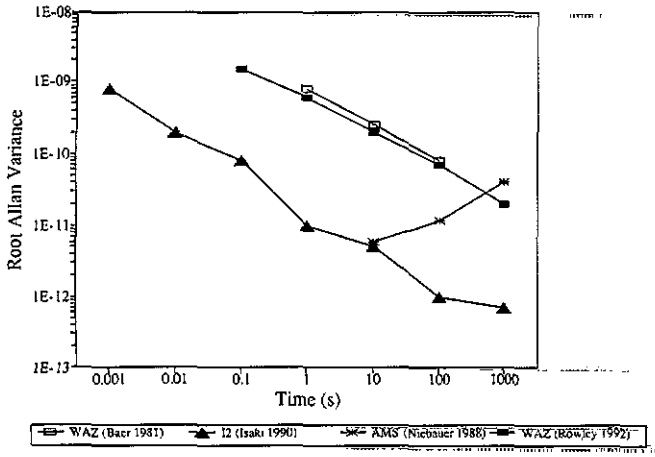


**Figure 13.** Recent short term frequency stability data for three types of stabilized He–Ne lasers. The stabilization principles for the weak axial field Zeeman laser (WAZ), the axial mode stabilized laser (AMS) and the iodine-locked laser (I2) are discussed in the text.

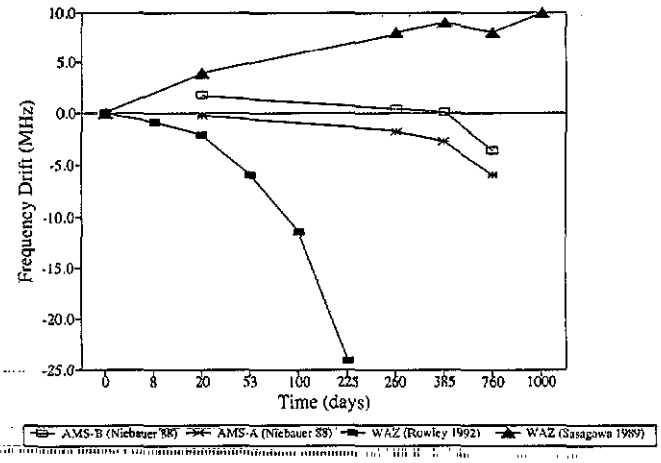


**Figure 14.** Recent long term frequency stability data for the weak axial field Zeeman laser (WAZ) and the axial mode stabilized laser (AMS).

a $\tau^{-1}$ dependence for $\tau$ greater than the servo time constant. This behaviour corresponds to white noise in the laser phase.

Recent stability data are summarized in figure 13. In the axial mode stabilized laser (AMS), the lock signal is proportional to the intensity difference between two axial modes. The weak axial field Zeeman laser (WAZ) derives a stabilization signature from the interstate beat frequency. Additional explanation of these stabilization techniques is found in section 5.3 in the context of long term stability. The iodine stabilized system (I2) is locked to an iodine absorption feature, as discussed in section 5.4. The short term performance of figure 13 is adequate for most interferometric applications. The WAZ data show an increase in Allan variance at very long times. This behaviour is somewhat atypical of published laser stability data and merits additional study. The stability of the iodine-locked laser exceeds that of other techniques by nearly two orders of magnitude. The $\tau^{-1}$ decrease in frequency stability at short times is a consideration in certain high-bandwidth applications. For example, the data rate in electron beam lithography may exceed 10 MHz. The bandwidth at which the stage interferometer feeds corrections into the deflection coils should be limited to the response of the mechanical system. This prevents high-frequency noise in the laser stability from being introduced to the writing process.

### 5.3. *Long term frequency stability*

The long-term behaviour of gain-curve-stabilized lasers is not as well characterized as the short term stability. Measurements from the recent literature are summarized in figure 14. The notation for the types of frequency control follows that of section 5.2 and figure 13. Only the study of Rowley, based on the weak axial field Zeeman laser (WAZ), clearly parametrizes the frequency as a function of the running hours of the tube. The remaining studies show frequency as a function of the combined shelf-life and running time. Consequently, the frequency drift data of Rowley appear steeper on this plot than that of the other studies.

Niebauer *et al* (1988) studied several laser tubes produced by a single manufacturer. These lasers are stabilized by equalizing the intensity of two axial cavity modes (Balhorn *et al* 1972). The modes are separated by 600 MHz for a 250 mm cavity, and oscillate in orthogonal linear polarizations. Because of the separation between the modes, they tend to oscillate at the edges of the gain curve (see figure 12). Radiation from one of the two modes is used in the single-frequency interferometer. In principle, equalizing the power in each mode keeps the cavity tuned to the centre of the gain curve. However, modes at the edges of the gain curve exhibit a less predictable response to changes in the laser gas parameters than do those at the centre. The individual shifts of the lower (red) and higher (blue) frequency modes are monitored in the study. Figure 14 shows the blue mode data (AMS-B) and average of red and blue modes (AMS-A). The mode spacing increases by about 2 MHz during the first two months of operation. The blue lock point shifts to higher frequency, while the red lock point decreases. The average frequency decreases with a slope equal to the long term value of 3–5 MHz per year. Niebauer *et al* use the average slope as a measure of predictability of stabilization. It is more relevant to consider the individual lock points, as only one mode is used in an interferometer. The blue mode in one laser increased by 3 MHz and did not return to the starting point for about two years. More research is necessary to explain these drifts. A drawback to the two-mode technique is the low output power which results from the edge of the gain curve. A complex variation of this scheme uses three modes, with one centred on the gain curve (Araki *et al* 1989).

In the weak axial field Zeeman laser, a longitudinal magnetic field of 0.005–0.02 tesla is applied to a single-cavity mode. The Zeeman effect splits the left and right circular polarization states into non-degenerate fre-

quency states, separated by about 100 kHz. Frequency pulling between states causes a minimum in beat frequency when the cavity is tuned to the centre of the transition line (Baer *et al* 1980). The precise behaviour of the tuning curve is determined by the field strength and Lamb dip profile (Rowley 1990). The long term performance of this stabilization technique may prove more predictable than axial mode stabilization (AMS) because the signal is derived from the centre rather than the edges of the gain curve. However, one experiment (Sasagawa and Zumberge 1989) shows a rapid increase in laser frequency, followed by a slow rise. This behaviour may be explained by a change in cavity dichroism.

In the transverse field Zeeman laser, a magnetic field is applied transverse to the cavity to produce a frequency split between the linearly polarized states. As with the weak axial field, the beat frequency depends on the cavity tuning. However, the tuning curve has a linear slope through the line centre rather than a minimum, and it is not necessary to dither the cavity (Morris *et al* 1975, Umeda *et al* 1980). The intermode beat frequency is locked to a local oscillator, and the laser can be tuned over a range of 250 MHz. The error signal between the intermode beat and local oscillator provides an audio frequency detuning signature. The audio error signal is particularly useful in identifying sources of frequency destabilization such as stray magnetic fields and optical feedback. Transverse and weak axial field Zeeman lasers are capable of single-state output powers from 1–3 mW because they operate near the centre of the gain curve.

The strong field axial Zeeman laser is the most widely used source for heterodyne interferometry in the 1–3 MHz range. In this system, the intensity difference between states is used to stabilize the wavelength. The maximum interferometer target velocity is limited by intermode beat frequency, which should exceed the Doppler shift of the interferometer target. A 1 MHz Doppler shift corresponds to a velocity of 150 mm $s^{-1}$ for a plane mirror interferometer. It is difficult to achieve a high split frequency in this type of laser. The separation of the transition frequencies caused by the Zeeman effect is about 850 times the change in index which determines the split in cavity modes. Furthermore, frequency pulling works to limit the intermode split for high cavity quality. Lasers with a split frequency of about 3 MHz and an output power of 400 $\mu$W have become available (Hewlett Packard model 5527C). Because the states oscillate on the edges of the gain curve, the laser frequency is sensitive to changes in the gain curve as in the axial mode stabilization (AMS) method.

### 5.4. Frequency stabilization to an external transition

Stabilization to an external reference, typically a narrow absorption feature, provides the greatest repeatability. Saturated absorption by an intracavity cell of low-pressure $^{127}I_2$ vapour is used at the He–Ne 633 nm line. The cavity is dithered across a hyperfine absorption feature, and the third derivative of the laser output power provides a tuning signal (Layer 1980). A repeatability of $10^{-11}$ (5 kHz) is achieved which is largely independent of the shelf-life, operating hours and ambient environment. This frequency resolution represents $10^{-3}$ of the 3–5 MHz width of the hyperfine lines. Such high stability requires careful attention to the iodine pressure and temperature, as well as power-induced frequency shifts (Chartier *et al* 1976, Layer 1980, Chartier 1983, Iwasaki and Chartier 1989). The frequency of a He–Ne laser stabilized to the g or i hyperfine line of $^{127}I_2$ is presently accepted with a standard deviation of $1.6\times10^{-10}$ (Jennings *et al* 1983). Through a combination of improved measurement accuracy, and more complete specification of the laser properties, the adopted uncertainty is likely to be reduced to $2.5\times10^{-11}$ in the near future (General Conference on Weights and Measures, CCDM Document 1992–19a). The frequencies of the g and i iodine hyperfine lines corresponding to this latest work are given in table 5. $^{127}I_2$ stabilization provides a wavelength standard traceable to the international length standard adopted by the General Conference on Weights and Measures in 1983. Traceability results from definition of the vacuum wavelength in terms of frequency $\lambda_v = c/f$. The velocity of light in vacuum $c$ is exactly 299 792 458 m $s^{-1}$.

The iodine-stabilized laser is not generally used directly for interferometry because of its low output power. A high-power traceable source is provided by frequency-locking a high-power He–Ne laser to the iodine-stabilized laser. The inter-laser beat signal is a servo signature to the high-power He–Ne laser. This approach is taken for the multi-axis interferometer on the large-optics diamond turning machine (LODTM) at Lawrence Livermore National Laboratory (Donaldson and Patterson 1983).

Dye lasers and diode lasers can also be stabilized to external transitions. The gain curves of these sources overlap a greater number of atomic transitions than gas lasers. By selecting a transistion which is much narrower than iodine, it may be possible to produce much better frequency standards. For example, an atomic beam of calcium has an absorption feature at 657 nm of 400 Hz linewidth. Frequency standards based on this approach are reviewed by Helmcke *et al* (1989).

### 5.5. Optical feedback and isolation

Optical feedback of light from the interferometer optics back into the laser is a major factor in short term frequency and intensity stability (Brown 1981, Hocken and Layer 1979, Smith 1973). Optical feedback is often difficult to identify and isolate. Feedback which is less than $10^{-6}$ in intensity can destabilize a gas laser. The error signal of the wavelength stabilization servo controller can be used to identify feedback. However, this signal is only available in usable form on a few commercial lasers (such as Laboratory for Science, Model 220, Berkeley, CA). Optical isolation of the laser is important and the most common methods are illustrated in figure 15. The linear polarizer and quarter-wave plate of figure 15(*a*) convert the laser output to circular polariz-

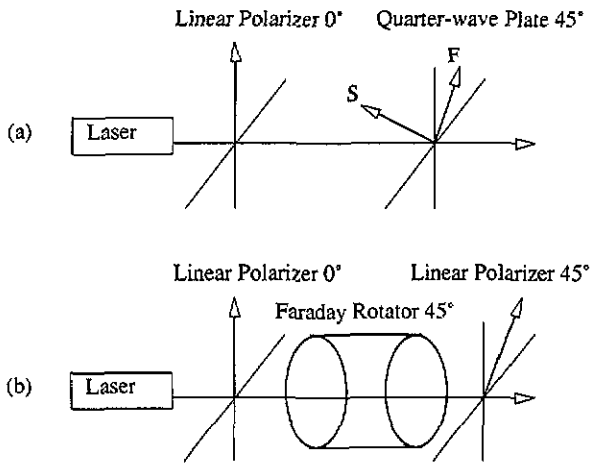


**Figure 15.** (*a*) A laser feedback isolator based on a combination linear polarizer and quarter-wave plate. (*b*) Better isolation is achieved by a Faraday rotator situated between an input and output linear polarizer.

ation. The circularly polarized component of the backscattered light is converted into the orthogonal linear polarization by the quarter-wave plate and is rejected. Because of imperfections in the optics, the intensity rejection ratio of this type of isolation is only about 0.01 for back reflections whose polarization state is unchanged. This method is ineffective when the interferometer optics modify the polarization of the return reflections. The method is found in the receivers of some commercial heterodyne interferometers where a quarter-wave plate is placed after the linear polarizer mixer to minimize reflections from the photodiode (such as Hewlett Packard model 10780). Better isolation is achieved with the Faraday rotator of figure 15(*b*). The Faraday effect rotates the linearly polarized input by 45°. The light passes through the output polarizer whose axis is oriented at 45°. Light returning through the Faraday isolator is rotated an additional 45° and is rejected by the polarizer. Rejection of $10^{-4}$ of the return intensity is typical.

Neither of the above isolation techniques is useful for the two-frequency and orthogonal polarization mode lasers used in heterodyne interferometry. A more general approach is frequency shift isolation (Smith 1973, Hocken and Layer 1979). The laser beam is passed through an acousto-optic modulator which shifts the optical frequency by about 100 MHz before it enters the interferometer optics. Light returning to the cavity experiences a second frequency shift from the acousto-optic modulator. The return light is mismatched to the cavity by 200 MHz. This approach is successfully incorporated in the interferometry system for the large-optics diamond turning machine at Lawrence Livermore Laboratory (Donaldson and Patterson 1983). The acousto-optic isolator can also be used to stabilize the intensity of the laser output by varying the drive power (Layer 1979).

### 5.6. Diode lasers for metrology

Development efforts in diode lasers are extremely intense. The driving applications are communications and optical storage with an emphasis on reliability, power and low cost. The properties of diode lasers and their use in displacement interferometry are reviewed by Abou-Zeid (1989). A GaAlAs 780 nm laser has an output power as large as 50 mW. The coherence length exceeds 20 m. The selection and wide range of wavelengths available from these devices are the basis of their advantages and drawbacks. The wavelength is extremely sensitive to the diode current and temperature. With current and temperature control, a stability of about $10^{-6}$ is achieved over a few days. Better stability requires the complexity of a Fabry–Pérot or transition lock, which makes the diode laser uncompetitive with the He–Ne 633 nm line for most commercial applications. The high power of the diode laser may be advantageous in overcoming the large coupling losses in interferometers which employ fibre optics.

The high gain of diode lasers makes them very sensitive to optical feedback. The feedback should be less than $10^{-8}$ in intensity (McInerney 1990). This is a particular problem when coupling into a fibre optic. It is difficult to fabricate an antireflection coating on a fibre which reflects less than $10^{-2}$ of the incident intensity. A Faraday-effect isolator is often employed in this situation. Further reduction of backscattered light is achieved by polishing a slant onto the end of the fibre optic. The effect of feedback on frequency can be modelled, and even used to advantage for some types of sensor (de Groot and Gallatin 1989). Diode lasers are primarily used in small displacement sensors (Waters and Fernald 1989) and two-wavelength absolute distance interferometry (de Groot 1991, Beheim 1986).

## 6. Resolution-extending electronics

The resolution of the interferometer is usually extended by electronic fringe interpolation. Although most measurements are performed with target velocities less than a few fringes per second, the electronics cannot lose track of the integer portion of the fringe count when the target is slewing between measurement locations. A plane mirror target velocity of 150 mm $s^{-1}$ corresponds to $10^6$ fringes per second. In a heterodyne interferometer, the phase detection circuitry operates at high frequency, even with a stationary target. Achieving high bandwidth at high resolution places considerable burden on the electronics. Applications such as lithographic pattern generation and reduction scanning printers (such as Micrascan, SVGL Corporation Wilton, CN), also require dynamic accuracy. The delay between the internal update of the fringe fraction and the transfer of data to the control system must have low jitter.

Validating the accuracy of the fringe interpolation system is difficult, especially for phase meters used in heterodyne interferometry. The beat frequency often

exceeds 2 MHz, and traceable electronic phase standards have only been available to about 40 kHz. One solution is to use a local oscillator and balanced RF mixers to shift the measurement and reference beat signals to lower frequencies. Recently, the National Institute of Standards and Technology (NIST) extended phase standards and calibration services to 20 MHz. The standards are accurate to about 0.03° at 250 kHz and 0.2° at 20 MHz. The new standards have been applied to the evaluation of several commercial high-frequency phase meters (Oldham *et al* 1993). It is important to note that accuracy must be verified at a high density of phase intervals, preferably at every resolution element of fringe subdivision. Some phase meters in my laboratory exhibit large errors which are localized to a small phase region. For example, a meter with subdivisions every 3° may be in error by ±13° at divisions between 30° and 40°, but accurate to 6° at every other phase subdivision. Localized errors are usually associated with discontinuities, such as a rising or falling edge, of the measurement, reference or clock signals.

Calibration of single-frequency interferometers is straightforward. The phase and amplitude relation of the quadratures can be accurately determined by digitizing the signals at low fringe rates. Once these parameters are established, the correction of computed phase for deviations of the quadrature phase from 90° is straightforward (Heydemann 1981). If dynamic accuracy is required, the performance at high fringe rate is derived from the low-rate data and the transfer function of the electronics.

Development activity is concentrated on phase meters for heterodyne interferometers. The most widely used types of phase meter are summarized by Oldham *et al* (1993). Time interval analysers, based on a combination of digital clocking and analogue interpolation, achieve accurate measurement at very high resolution. However, they have low update rates and consequently lose track of the integer portion of the fringe count during rapid slewing of the target. The resolution–bandwidth product of this type of phase meter is insufficient for high-speed stage applications. This limitation can be overcome using a coarse fringe counter during rapid target motion and a high-resolution phase meter during quasi-static measurement (Mori *et al* 1988). Analogue interpolation between clock cycles of a time interval analyser can be replaced by a delay line with $N$ taps. Each tap produces a copy of the clock phase shifted by $2\pi/N$, which is latched to interpolate $N$ points between clock cycles. The delay line principle permits a rapid update rate and works with a heterodyne frequency of 10 MHz. A time stamp is also latched with each phase update so that the dynamic accuracy is not affected by delays in transferring the data out of the phase meter (Zygo Model ZMI-1000). It is also possible to accomodate a target velocity whose Doppler shift exceeds the heterodyne frequency by detecting this condition electronically and continuing to track the phase shifted frequency (Yokoyama *et al* 1990).

Phase meter electronics are usually placed outside the thermally stabilized metrology environment. Consequently, the design must be compensated and evaluated for thermal sensitivity.

**Table 6.** Other laser lines.

| Laser line | $\lambda$ (nm) |
|---|---|
| He–Ne (infrared) | 1300 |
| Nd : YAG (infrared) | 1060 |
| GaAlAs (infrared) | 780 |
| HeNe (orange) | 612 |
| HeNe (yellow) | 594 |
| HeNe (green) | 543 |
| Argon ion (blue) | 488 |

## 7. Summary and future prospects

Laser interferometry is used for a well-defined set of displacement measurements whose accuracy requirements exceed those of glass scale encoders. Performance in these applications will continue to be enhanced by improved control of the measurement environment. Direct improvements to the laser heads, interferometer optical systems and phase measuring electronics will also contribute to improved measurement accuracy and repeatability. The area of greatest potential change is for interferometers to replace the numerous applications which use glass scale and magnetic encoders. A compact interferometer which is competitive in cost with the scale encoders and accurate to better than $5\times10^{-6}$ of the measurement path is required. Several years ago, it was felt that interferometers based on the diode laser in combination with optical fibres would supplant scale encoders. Commercial development of low-cost diode laser interferometers for the machine tool industry has not advanced as rapidly as expected. The performance of scale encoders continues to improve, with costs remaining constant or decreasing. However, the market remains large, and the next ten years may see stronger competition of interferometers in applications presently dominated by optical and magnetic encoders.

## Acknowledgments

I would like to thank Tyler Estler, Jack Stone, Doug Goodman, Alan Rosenbluth, Bob Hocken, Mark Colavita, John Tsai, Michael Player, Peter de Groot, W R C Rowley, Michael Downs and Ned Bennett for their comments on this review.

## References organized by subject

### General

Babcock H W 1962 Control of a ruling engine by a modulated interferometer *Appl. Opt.* **1** 415–20

Baird E D, Patterson S R and Donaldson R R 1990 The laser interferometer for the large optics diamond turning machine, LLNL internal report
Beheim G 1986 Fiber-optic interferometer using frequency-modulated laser diodes *Appl. Opt.* **25** 3469–72
Bobroff N 1993 Critical alignments in plane mirror interferometry *Precision Eng.* **15** 33–8
Charette P G, Hunter I W and Brenan C J H 1992 A complete high performance heterodyne interferometer transducer for microactuator control *Rev. Sci. Instrum.* **63** 241–8
de Groot P 1991 Interferometric laser profilometer for rough surfaces *Opt. Lett.* **16** 357–9
Donaldson R R and Patterson S R 1983 Design and construction of a large, verticle axis diamond turning machine *Proc. SPIE* **433** 62–7
Association of German Engineers 1985 Laser interferometry in length measurement (Dusseldorf: VDI) pp 1–121
Estler W T and Megrab E B 1985 Validation metrology of the large optics diamond turning machine, NBSIR 85-3182(R) NIST internal report
Hariharan P 1987 Interferometry with lasers *Progress in Optics* vol 24 ed E Wolf (Amsterdam: Elsevier) pp 108–64
Hines B, Colavita M, Wallace K and Poulsen A 1992 Sub-nanometer laser metrology – some techniques and models *High resolution imaging by interferometry II, Garching*. ed J M Beckers and F Merkle (ESO) Conference and Workshop Proceedings, vol 39, pp 1195–204
Kendall R, Doran S and Weissmann E 1991 A servo guided *X–Y*-theta stage for electron beam lithography *J. Vac. Sci. Technol.* B **9** 3019–23
Kennedy R J 1926 A refinement of the Michelson–Morley experiment *Proc. NAS* **12** 621–9
Michelson A A and Morley E W 1887 On the relative motion of the earth and the luminiferous ether *Phil. Mag.* **24** 449–63
Monchalin J P, Kelly M J, Thomas J E, Kurnit N A, Szoke A, Zernike F, Lee P H and Javan A 1981 Accurate laser wavelength measurement with a precision two-beam scanning Michelson interferometer *Appl. Opt.* **20** 736–56
Schussler H H 1985 Comparison and calibration of laser interferometer systems *Measurement* **3** 175–84
Steinmetz C R 1990 Sub-micron measurement and control on precision machine tools with laser interferometry *Precision Eng.* **12** 12–24
Wagner J W and Spicer J B 1987 Theoretical noise-limited sensitivity of classical interferometry *J. Opt. Soc. Am.* B **4** 1316–26
Waters J P and Fernald M R 1989 Pocket-size interferometric systems *Proc. SPIE* **1162** 16–25

## Interferometer optics

Baldwin R R and Siddall G J 1984 A double pass attachment for the linear and plane mirror interferometer *Proc. SPIE* **480** 80–7
Cummings A L and Hocken R J 1982 An accurate temperature-controlled polarimeter *Precision Eng.* **4** 33–8
Downs M J 1990 A proposed design for an optical interferometer with sub-nanometer resolution *Nanotechnology* **1** 27–30
Downs M J and Raine K 1979 An unmodulated bidirectional fringe-counting interferometer for measuring displacement *Precision Eng.* **1** 25–88
Hines B, Shao M, Colavita M M and Staelin D H 1990 Use of laser metrology optical truss for monitoring baseline motion *Proc. SPIE* **1237** 87–99
King R J and Talim S P 1971 Some aspects of polarizer performance *J. Phys. E: Sci. Instrum.* **4** 93–6
Lichten W 1985 Precise wavelength measurements and optical phase shifts I. General theory *J. Opt. Soc. Am.* A **2** 1869–76
Player M A 1988 Polarization properties of a cube-corner reflector *J. Mod. Opt.* **35** 1813–20
Sommargren G E 1987 A new laser measurement system for precision metrology *Precision Eng.* **9** 179–84
——1989 Linear/angular displacement interferometer for wafer stage metrology *Proc. SPIE* **1088** 268–72

## Environment

Beers J and Doiron T 1993 Verification of revised water vapour correction to the index of refraction of air *Metrologia* **29** 315–6
Birch K P and Downs M J 1988 The results of a comparison between calculated and measured values of the refractive index of air *J. Phys. E: Sci. Instrum.* **21** 694–5
——1989 Error sources in the determination of the refractive index of air *Appl. Opt.* **28** 825–6
Birch K P, Downs M J and Ferriss D H 1988a Optical path length changes induced in cell windows and solid etalons by evacuation *J. Phys. E: Sci. Instrum.* **21** 690–2
Birch K P, Downs M J and Ward R E 1988b The measurement of humidity variation in gases resulting from the adsorption of water on to surfaces *J. Phys. E: Sci. Instrum.* **21** 692–4
Bobroff N 1987 Residual errors in laser interferometry from air turbulence and nonlinearity *Appl. Opt.* **26** 2676–81
Downs M J, Ferriss D H and Ward R E 1990 Improving the accuracy of the temperature measurement of gases by correction for the response delays in thermal sensors *J. Meas. Sci. Technol.* **1** 1–3
Edlen B 1966 The refractive index of air *Metrologia* **2** 71–80
Estler W T 1985 High accuracy displacement interferometry in air *Appl. Opt.* **24** 808–15
Hohm U and Kerl K 1990 A Michelson twin interferometer for precise measurements of the refractive index of gases between 100 K and 1300 K *Meas. Sci. Technol.* **1** 329–36
Ishida A 1989 Two-wavelength displacement-measuring interferometer using second-harmonic light to eliminate air-turbulence-induced errors *Japan. J. Appl. Phys. Lett.* **28** 473–5
Jones F E 1980 The refractivity of air *J. Res. Nat. Bur. Standards* **96** 27–32
Matsumoto H, Zhu Y, Iwasaki S and O'ishi T 1992 Measurement of the changes in air refractive index and distance by means of a two-color interferometer *Appl. Opt.* **31** 4522–6
Pace C F 1989 Non-catastrophic failure of the laser transducer system in a universal measuring machine *Precision Eng.* **11** 239–41
Popela B 1972 He–Ne laser and the solution of corrections of the laser interferometer *Acta* **19** 606–12
Ruth J H 1986 Thresholds and irritation levels of several chemical substances *Am. Ind. Hyg. Assoc. J.* **47** A142–51
Schellekens P, Wilkening G, Reinboth F, Downs M J, Birch K P and Spronck J 1986 Measurements of the refractive index of air using interference refractometers *Metrologia* **22** 279–87
Slater L E and Huggett G R 1976 A multiwavelength distance-measuring instrument for geophysical experiments *J. Geophys. Res.* **81** 6299–306
Steinmetz C R 1988 Displacement measurement repeatability in tens of nanometers with laser interferometry *Proc. SPIE* **921** 406–20
Weichel H 1990 *Laser Beam Propagation in the Atmosphere* (Society of Photo-optical Instrumentation Engineers)
Wood S D, Mangum B W, Filliben J J and Tillett S B 1978

An investigation of the stability of thermistors *J. Res. Nat. Bur. Standards* **83** 247–63

### asers for interferometry

.bou-Zeid A 1989 Diode lasers for interferometry *Precision Eng.* **11** 139–44
Allan D W 1966 Statistic of atomic frequency standards *Proc. IEEE* **54** 221–30
Araki T, Nakajima Y and Suzuki N 1989 Frequency and intensity stabilization of a high output power, internal mirror He–Ne laser using interferometry *Appl. Opt.* **28** 1525–8
Baer T, Kowalski F V and Hall J L 1980 Frequency stabilization of a He–Ne longitudinal Zeeman laser *Appl. Opt.* **19** 3173–7
Balhorn R, Kunzmann H and Lebowsky F 1972 Frequency stabilization of internal-mirror helium–neon lasers *Appl. Opt.* **11** 742–4
Balhorn R, Lebowsky R and Ullrich D 1975 Beat frequency between two axial modes of He–Ne laser with internal mirrors and its dependence on cavity *Q Appl. Opt.* **14** 2955–9
BIPM 1984 Documents concerning the new definition of the metre *Metrologia* **19** 163–78
Brown N 1981 Frequency stabilized lasers: optical feedback effects *Appl. Opt.* **20** 3711–4
Chartier J-M 1983 Results of international comparisons *using methane-stabilized HeNe lasers at 3.39 μm and* iodine-stabilized HeNe lasers at 633 nm *IEEE Trans. Instrum. Meas.* **32** 81–3
Chartier J-M, Darnedde H and Frennberg H M 1992 International comparisons of northern European iodine stabilized HeNe lasers at 633 nm *Metrologia* **29** 331–9
Chartier J-M, Helmeke J and Wallard A J 1976 International intercomparison of wavelength of iodine-stabilized lasers *IEEE Trans. Instrum. Meas.* **25** 450–3
Chartier J-M, Robertsson L and Sommer M 1991 International comparisons of iodine stabilized HeNe lasers at 633 nm involving seven laboratories *Metrologia* **28** 19–25
Ciddor P E and Duffy R M 1983 Two-mode frequency-stabilized He–Ne lasers: studies of short-and-long-term stability *J. Phys. E: Sci. Instrum.* **16** 1223–7
de Groot P J and Gallatin G M 1989 Backscatter-modulation velocimetry with an external-cavity laser diode *Opt. Lett.* **14** 165–7
Helmcke J, Morinaga A, Ishikawa J and Riehle F 1989 Optical frequency standards *IEEE Trans. Instrum. Meas.* **38** 524–32
Hocken R J and Layer H P 1979 Laser for dimensional measurement *Ann. CIRP* **28** 303–6
Holzapfel W, Luxem W and Settgast W 1990 Stabilization of single frequency internal mirror He–Ne lasers: comment *Appl. Opt.* **29** 3877–8
Iwasaki S and Chartier J M 1989 Comparison of iodine stabilized HeNe lasers at 633 nm wavelength *Metrologia* **26** 257–61
Jennings D A, Pollock C R, Petersen F R, Drullinger R E, Evenson K M and Wells J S 1983 Direct frequency measurement of $I_2$-stabilized He–Ne 473-THz (633-nm) laser *Opt. Lett.* **8** 136–8
Koning J, Schellekens P H J and McKeown P A 1979 Wavelength stability of He–Ne lasers used in interferometry – limitations and traceability *Ann. CIRP* **28** 307–10
Layer H P 1979 Acoustooptic modulator intensity servo *Appl. Opt.* **18** 2947–9
Layer H P 1980 A portable iodine stabilized helium neon laser *IEEE Trans. Instrum. Meas.* **29** 358–61
McInerney J G 1990 Low-frequency intensity fluctuations in external cavity semiconductor lasers *Proc. SPIE* **1376** 236–43
Morris R H, Ferguson J B and Warniak J S 1975 Frequency stabilization of internal mirror HeNe lasers in a transverse magnetic field *Appl. Opt.* **14** 2808
Niebauer T M, Godwin H M, Faller J E, Hall J L and Barger R I 1988 Frequency stability measurements on polarization stabilized He–Ne lasers *Appl. Opt.* **27** 1285–9
Pan C-L, Jean P-Y, Kuo C-C, Hsieh T-C and Lei T F 1985 Sensitivity of frequency stability of two-mode internal-mirror He–Ne lasers to misalignment of polarizing optics *Appl. Opt.* **24** 3430–1
Puntambekar P N, Mohanty P K and Dahiya H S 1987 Frequency stabilization of 633 nm HeNe laser using polarization modulation *IEEE Trans. Instrum. Meas.* **36** 636–8
Rowley W R C 1990 The performance of a longitudinal Zeeman stabilised He–Ne laser with thermal modulation and control *Meas. Sci. Technol.* **1** 348–51
Sasagawa G S and Zumberge M A 1989 Five year frequency stability of a Zeeman stabilized laser *Appl. Opt.* **28** 824–5
Sasaki A, Wakabayashi K and Masuda S-I 1989 Stabilization of single frequency internal mirror He–Ne laser *Appl. Opt.* **28** 1608–9
Smith R G 1973 Use of acoustooptic light deflector as an optical isolator *IEEE J. Quant. Electron.* **9** 545–6
Takasaki H, Umeda N and Tsukiji M 1980 Stabilized transverse Zeeman laser as a new light source for optical measurement *Appl. Opt.* **19** 435–41
Tobias I, Skolnick M L, Wallace R A and Polanyi T G 1965 Derivation of frequency-sensitive signal from gas laser in an axial magnetic field *Appl. Phys. Lett.* **6** 198–200
Umeda N, Tsukiji M and Takasaki H 1980 Stabilized He–Ne transverse Zeeman laser *Appl. Opt.* **19** 442–50
Wallard A J 1973 Frequency stabilization of gas lasers *J. Phys.* **6** 793–807
Xie Y and Wu Y 1989 Elliptical polarization and nonorthogonality of stabilized Zeeman laser output *Appl. Opt.* **28** 2043–6
Zumberge M A 1985 Frequency stability of a Zeeman-stabilized laser *Appl. Opt.* **24** 1902–4

### Nonlinearity

Augustyn W and Davis P 1990 An analysis of polarization mixing errors in distance measuring interferometers *J. Vac. Sci. Technol.* B **8** 2032–6
Bobroff N 1987 Residual errors in laser interferometry from air turbulence and nonlinearity *Appl. Opt.* **26** 2676–81
Bruning J H, Herriott D R, Gallagher J E, Rosenfield D P, White A D and Brangaccio D J 1974 Digital wavefront measuring interferometer for testing optical surfaces and lenses *Appl. Opt.* **13** 2693–703
Fedotova G V 1980 Analysis of the measurement error of the parameters of mechanical vibration *Meas. Techniques* **23** 577–80
Hou W and Wilkening G 1992 Investigation and compensation of the nonlinearity of heterodyne interferometers *Precision Eng.* **14** 91–8
Korneev V J 1985 Transfer function of an optical system *with a corner reflector Opt. Spectrosc.* **58** 407–9
Lamekin P I 1988 Polarization properties of corner reflectors *Sov. J. Opt. Technol.* **55** 16–9
Quenelle R C 1983 Nonlinearity in interferometer measurements *Hewlett Packard J.* **34** 10
Rosenbluth A E and Bobroff N 1990 Optical sources of nonlinearity in heterodyne interferometers *Precision Eng.* **12** 7–11

Sommargren G E 1987 A new laser measurement system for precision metrology *Precision Eng.* **9** 179–84
Sutton C M 1987 Non-linearity in length measurement using heterodyne laser Michelson interferometry *J. Phys. E: Sci. Instrum.* **10** 1290–2
Tanaka M, Yamagami T and Nakayama K 1989 Linear interpolation of periodic error in a heterodyne laser interferometer at subnanometer levels *IEEE Trans. Instrum. Meas.* **38** 552–4
Yi Xie and Yi-zun Wu 1992 Zeeman laser interferometer errors for high-precision measurements *Appl. Opt.* **31** 881–4

## Electronics

Downs M J and Raine K W 1979 An unmodulated bi-directional fringe-counting interferometer system for measuring displacement *Precision Eng.* **1** 85–88
Hagiwara N, Nishitani Y, Yanase M and Saegusa T 1989 A phase encoding method for improving the resolution and reliability of laser interferometers *IEEE Trans.* **38** 548–51
Heydemann P L M 1981 Determination and correction of quadrature fringe measurement errors in interferometers *Appl. Opt.* **20** 3382–4
Mertz L 1983 Real-time fringe-pattern analysis *Appl. Opt.* **22** 1535–9
——1988 Complex homodyne reception from discrete photons *Appl. Opt.* **27** 3429–32
——1989 Optical homodyne phase metrology *Appl. Opt.* **28** 1011–4
Mori S, Akatsu T and Miyazaki C 1988 Laser measurement system for precise and fast positioning *Opt. Eng.* **27** 823–9
Oka K, Tsukada M and Ohtsuka Y 1991 Real-time phase demodulator for optical heterodyne detection processes *Meas. Sci. Technol.* **2** 106–10
Oldham N, Kramar J A, Hetrick P S and Teague E C 1993 Electronic limitations in phase meters for heterodyne interferometry *Precision Eng.* **15**
Wagner J W and Spicer J B 1987 Theoretical noise-limited sensitivity of classical interferometry *J. Opt. Soc. Am.* B **4** 1316–26
Yokoyama S, Nishihara I, Okamoto A, Araki T and Suzuki N 1990 A high-speed and high-resolution heterodyne interferometer *Proc. SPIE* **1319** 212–3